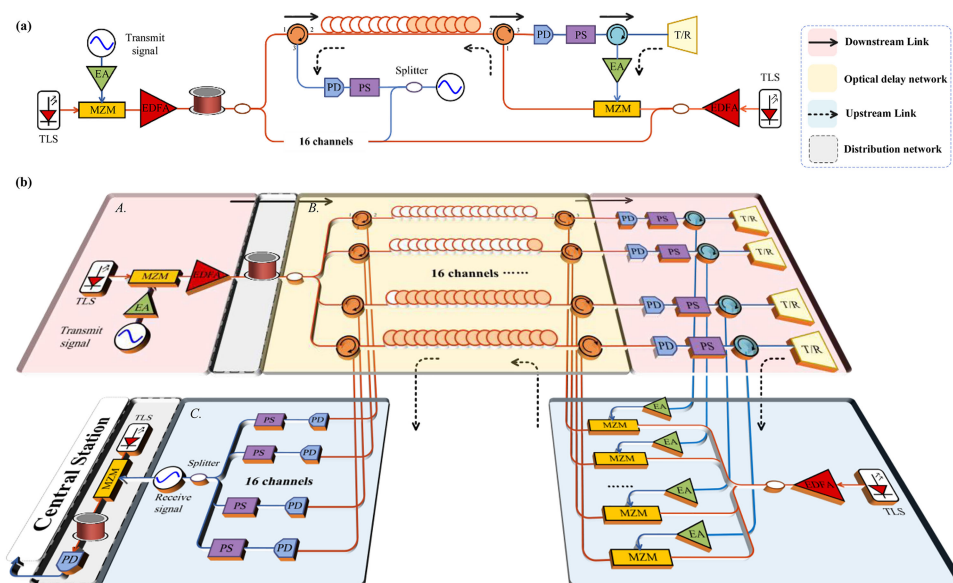# An Up/Downstream Shared Optical Beam Forming Network for Remote Phased Array Antenna

Yao Meng
Ye Xiao
Wei Li, *Member, IEEE*
Nuannuan Shi
Ming Li

An Up/Downstream Shared Optical Beam Forming Network for Remote Phased Array Antenna

Yao Meng [1,2,3] **Ye Xiao** [1,2,3] **Wei Li** [1,2,3] *Member, IEEE*, **Nuannuan Shi** [1] **and Ming Li** [1,2,3]

[1]State Key Laboratory on Integrated Optoelectronics, Institute of Semiconductors,Chinese Academy of Sciences, Beijing 100083, China
[2]School of Electronic, Electrical and Communication Engineering, University of Chinese Academy of Sciences, Beijing 100049, China
[3]Center of Materials Science and Optoelectronics Engineering, University of Chinese Academy of Sciences, Beijing 100190, China

Abstract: An up/downstream shared optical beam forming network based on wavelength-swept for remote phased array antenna is presented and experimentally demonstrated. A shared optical true time delay (TTD) network minimizes the size and cost, which is made by 16 paths of variable lengths of dispersion compensation fibers splicing with single-mode fiber, and then corporate with optical circulators. The experimental results show that the proposed system provides wide bandwidth from 12 GHz to 17GHz. The main lobe is oriented from $-49.3°$ to $45.9°$ and the spurious free dynamic range (SFDR) of 104.58 dB·Hz$^{2/3}$ is achieved in this system. Besides, the optical beam forming network is not affected by external temperature interference. This structure could have applications in remote phased array antenna.

Index Terms: Microwave photonics, Beam steering, Phased arrays.

1. Introduction

With the increasing mission of the modern information operation, it is an urgent need for the industry and academia to exploit the new institutional radar, which is desired to meet the requirement of the multi-functional wideband coverage and effective connection of the front-end distributed wideband antenna with the back-end signal processing unit. In general, the conventional digital synthesis technique for broadband beam forming needs to undergo a serial of analog signal processing including frequency-conversion, filter, channelization, etc. [1], [2]. It involves the difficulty that the electronic device is hard to support the digitization of ultra-wideband (UWB) signal. Moreover, the coaxial-cable for the long haul does not maintain the amplitude consistence of the UWB signal and more seriously introduce the loss up to several hundreds dB per kilometer. The microwave photonics technology, which combines the technological superiority of the photonic and the

microwave, is an optimized alternative. The low loss performance of optical fiber used for the long haul and microwave technology is applied to the flexible configuration. The analog synthesis technique for remote phased array antenna (PAA) can be realized.

The optical beam forming networks used for the remote PAA, as the main component in the new institutional radar, has attracted wide interest for the past decades. The true time delay (TTD) technology, compared with the electronic time delay technology such as phase shifter, has been demonstrated within a less beam squint over a larger instantaneous bandwidth [2]–[5]. Optical delay lines instead of electronic phase shifter have been designed by incorporating the optical fiber with the optical switching [6], [7], fiber grating [8], [9], dispersive medium [10]–[12], etc. Ref. [12] reported an X-band dispersion compensation fiber (DCF)–based phased array radar with the bandwidth from 8 to 12 GHz and the main lobe is oriented from $0°$ to $\pm 54°$. A separate receiving antenna is used to measure the performance of the transmitting beamforming. However, in transceiver phased array radar, the beam forming technique is used on both transmit and receive end that allows the power of transmit and receive signal much more concentrated on the assigned orientation so the angle resolution could be increased. While the reported optical beam forming has demonstrated a large scanning angle, the optical beam forming for transmitting at the front end and receiving at the back end are separated with each other, which uses two sets of analogous optical delay networks. It introduces the difficulty of the collaborative control of the transmit and receive optical delay networks due to the inconsistency in the fabrication of the optical delay line as well as influence difference of the external environment. Therefore, a common optical beam forming network with the up/downstream shared one TTD network can overcome these above challenges.

In this letter, we experimentally validate a wavelength-swept optical beam forming network for remote phased array antenna. The experimental results show that the proposed system provides wide bandwidth from 12 GHz to 17GHz. The main lobe is oriented from $-49.3°$ to $45.9°$ and the spurious free dynamic range (SFDR) of 104.58 dB·Hz$^{2/3}$ is achieved in this system. Besides, the optical beam forming network is not affected by external electromagnetic and temperature interference. This structure could have applications in remote phased array antenna, which is beneficial for cooperative control and flexible configuration. This optical beam forming network we proposed has potential applications in chip-scale integration in the future [13]–[17].

2. Principle

The schematic of the up/downstream shared optical beam forming network is represented in Fig. 1, which is divided into three-part, including the transmit front end, the shared optical delay network, and the receive back end. A transmit link in downstream is used to realize electronic-to-optical conversion and subsequently send to a few kilometers of optical fiber, an optical delay network as well as optical-to-electronic conversion. It consists of a tunable laser source (TLS), a Mach-Zehnder modulator (MZM), an electronic amplifier (EA), an erbium-doped fiber amplifier (EDFA), photodetectors (PDs), and phase shifters (PSs). An optical delay network with wavelength dispersion delay technology can realize true time delay, which is composed of the 16 rolls of self-design optical fiber delay lines and optical couplers (OCs). The OCs are used to share the optical delay network by the transmit and receive links, benefited the cooperative control of the whole system. A receiver link in upstream undergoes electronic-to-optical conversion, a shared optical delay network, and the optical-to-electronic conversion. Afterwards, the 16 paths microwave signals are combined into one path with an electronic combiner. The combination in the electronic domain rather than the optical domain reduces the power jitter caused by the optical interference. In addition, the structural design of the integrated transceiver saves considerable size and cost.

2.1 The Downstream Link

For the transmit front end, the light wave from the C-band TLS is modulated by the amplified transmit microwave signal via an MZM, amplified through an EDFA, and subsequently sent to a length of optical fiber to realize the distribution of the transmit signals to remote site antennas. Then the optical signal is launched into the optical delay network to get different delay times,
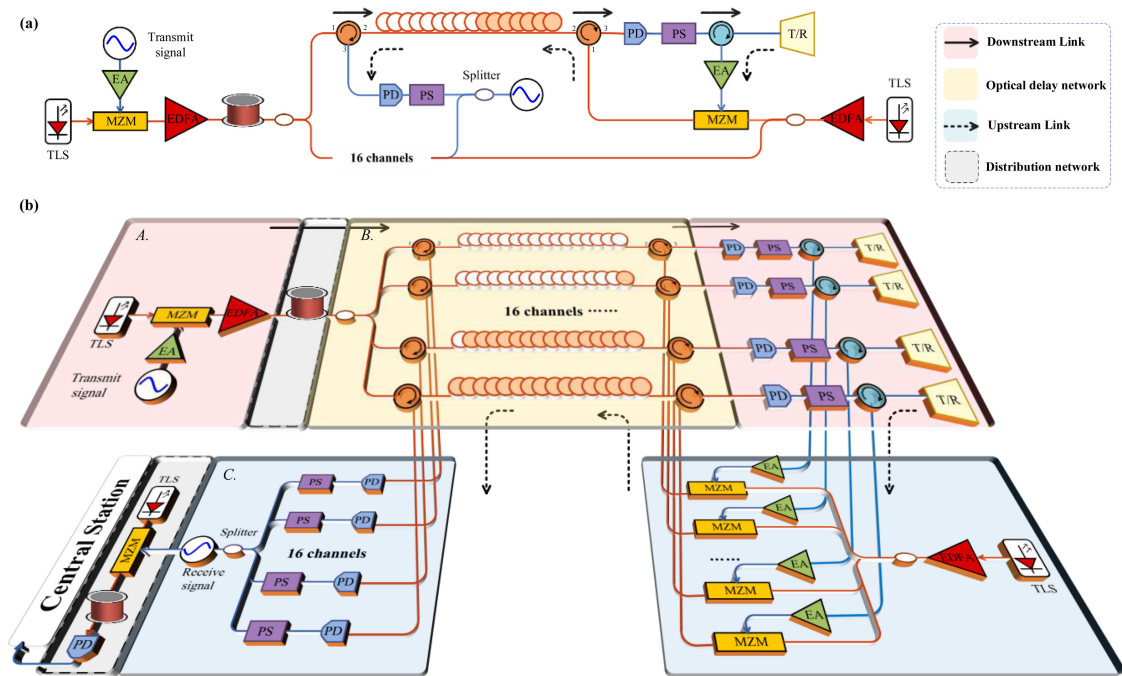
Fig. 1. The schematic of the up/downstream shared optical delay networks. (a) The schematic diagram of the whole system. (b) The detailed link figure of the proposed system. A is the downstream, B is the optical delay network, C is the upstream, and the gray parts are the distribution network. TLS: tunable laser source; MZM: Mach-Zehnder modulator; EDFA: erbium dropped fiber amplifier; OC: optical coupler; PD: photodetector; PS: phase shift; EA: electronic amplifier; T/R: transmit-receive modules.

since the different lengths of dispersion compensation fiber (DCF) in every channel. It is converted into microwave signals by separate PDs. The small errors of the signals' primary phases are compensated by PSs, to make sure the phase differences are zero in the central wavelength of light. The microwave signals are sent to free space by the transmit/receive (T/R) modules respectively.

Because of the difference of time delay between each channel, a particular direction of the beam forming is generated and determined by space interference. Specifically, assuming that the amplitudes and the initial time delays Δt between the adjacent channel are the same, the physical processes that 16-channel secondary wave sources are interfered in the free space after transmitting along 16 channels time delay lines and launch by 16 channels phased-array antenna as the equation can be expressed as

$$|E_a| = \left| \sum_{n=0}^{N-1} \sin \left[\omega_0 \left(t + n\Delta t \right) + n \frac{2\pi d}{\lambda_{RF}} \sin \theta \right] \right|$$

$$\alpha \left| E_a \left(\theta \right) \right| = \left| \frac{\sin \left[\frac{N}{2} \left(\omega_0 \Delta t + \frac{2\pi d}{\lambda_{RF}} \sin \theta \right) \right]}{\sin \left[\frac{1}{2} \left(\omega_0 \Delta t + \frac{2\pi d}{\lambda_{RF}} \sin \theta \right) \right]} \right| \tag{1}$$

Where N is the total number of elements, ω_0 is the angular frequency of the transmit signal, d represents the spatial distance between the adjacent transmitting antenna, λ_{RF} is the wavelength of the transmit signal, θ is the angle between the array elements normal direction and the beam direction. The total electric field strength E_a is a superposition of transmit signal of N channels, which can be written naturally as a function of θ. E_a takes the maximum at $\omega_0 \cdot \Delta t + \frac{2\pi d}{\lambda_{RF}} \sin \theta = 0$

corresponding to the scan angle. It shows that the directional diagram sweeps by changing the delay difference Δt of each channel.

2.2 The Shared Optical Delay Network

In the shared optical delay network, the transmit signal is divided and launched into 16 channels. The delay arrays are inserted before the array elements to change the phase difference between the adjacent elements, which can be expressed as 0, $d\sin\theta$, $2d\sin\theta$, …, $(N-1)d\sin\theta$. Hence, the arrival time of every element signals are unequal, which steered the element to different positions.

The key parameters in the shared optical delay network are the delay arrays of every channel. In the proposed system, the total delay of each channel is tunable with the wavelength of laser, so the dispersion coefficients and the fiber length need to be carefully designed. In the center wavelength of laser λ_0, the phase differences of each channel are zero, so the total fiber lengths are equal in each channel. In the designed maximum wavelength λ_m, the beam direction is pointed to the max angle θ_m. When the wavelength λ is fixed, the delay difference between the adjacent channels can be expressed as

$$\Delta t = D_{DCF} \cdot \Delta L \cdot \Delta\lambda + D_{SMF} \cdot (-\Delta L) \cdot \Delta\lambda \tag{2}$$

Where wavelength difference is $\Delta\lambda = \lambda - \lambda_0$, D_{DCF} and D_{SMF} are the dispersion coefficient, ΔL is the length change of DCF or SMF in the adjacent channel, which codetermined the time delay between channels. With the calculation and design of fiber length, the optical delay network is formed by the precise incremental delay time of 16 channels.

2.3 The Upstream Link

Similarly, the receive back-end module has the same fundamental as the transmit front-end module. To eliminate the interference of optical coupling in multi-channel-structure, the optical carriers need to transform long fibers which much beyond the coherence length before modulated. In the proposed system, the too-long fibers will reduce the stability, so the optical carriers are modulated again before combining them together. It is different from the transmit signal which is modulated before the split, for the receive module, the receive signals from the T/R modules are amplified and converted into the optical signal in 16 channels respectively. Then after the specific delays, the microwave signals are detected by PDs and combined all channels as one signal by a 1:16 combiner. It's worth noting that the signal combination is in the electric field rather than the light field, because the light is more sensitive to the perturbation that causes the coherent interfering signals cancellation phenomenon. The polarization-maintaining device including the TLS, the EDFA and the 1:16 optical coupler are used to reduce the polarization dependent loss and enhance the system stability. The two TLSs are symmetric about center wavelength of 1545 nm to make sure the quality of the receive signal. For further discussion, the receive signal can undergo an electronic-to-optical and an optical-to-electronic conversion again to process signals in the central station via the low-loss long fiber. This kind of antenna remoting solution based on microwave photonics can easily combine with the proposed system. The proposed remote phased array antenna system satisfies the processing requirement of high-frequency and large-bandwidth signals.

3. Results and Discussion

As illustrated in Fig. 1, the up/downstream link shared optical beam forming network consists of two TLSs (PPCL300) with a tunable step of 0.001 nm, 20-GHz MZMs (Oclaro AM-20), EDFAs (Keopsys) which can deliver up to 33 dBm of saturated output power, 20-GHz PDs (EM169), EAs (TLA8-20), two 1:16 optical splitters, optical circulators, PSs (BM12000), 16 rolls of custom optical fibers which the dispersion coefficient of DCF and SMF are 17 ps/nm and -140 ps/nm, electrical circulators, and an electrical combiner. To confirm the MZMs are biased at their optimum linear point

TABLE 1
The Designed Length of the Fibers in Each Channel

| Channel	1	2	3	4	5	6	7	8
Delay difference/ps	31.47	62.93	94.39	125.86	157.33	188.80	220.26	251.73
DCF/m	0.00	13.36	26.72	40.08	53.44	66.80	80.16	93.52
SMF/m	200.40	187.04	173.68	160.32	146.96	133.60	120.24	106.88
Channel	9	10	11	12	13	14	15	16
Delay difference/ps	283.19	314.66	346.13	377.59	409.06	440.52	471.99	503.46
DCF/m	106.88	120.24	133.60	146.96	160.32	173.68	187.04	200.4
SMF/m	93.52	80.16	66.80	53.44	40.08	26.72	13.36	0.00
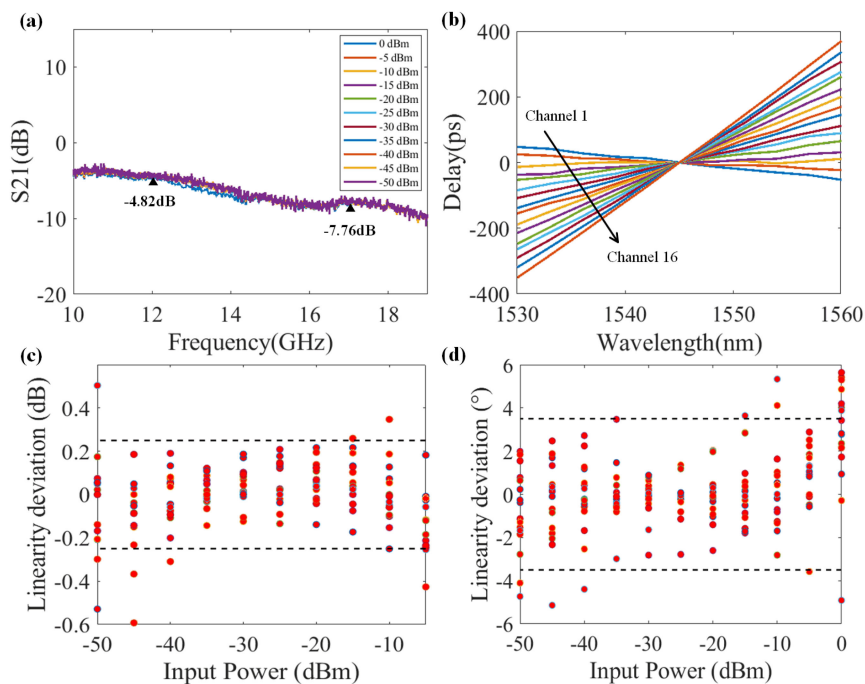
Fig. 2. (a) The S_{21} parameters of receive channel 5 at different input power. (b) The time delay curves for all 16 channels beamformer, when the first channel in 1545 nm is used as a reference. (c) The power linearity deviations in all receive-channels. (d) The phase random error in all transmit-channels.

with the temperature variation, every MZM is configured with a bias controller. Table 1 introduces the designed length of the fibers in each channel. The actual length and dispersion coefficient may have slight errors in fabrication and construction.

We measure and analyze the transmit signal of total 32 channels using S_{21} parameters by vector network analyzer (VNA). The 3dB-bandwidth, power loss per channel, liner area, and so on can be obtained by analyzing S_{21} parameters correspondingly.

3.1 Electrical Characteristics

The amplitude and phase information of S_{21} parameters can be processed to the 3 dB-bandwidth and delays. Taking the upstream channel 5 as a sample, the amplitude of S_{21} parameters every 5 dB under different input power from -50 dBm to 0 dBm are shown in Fig. 2(a). The results

show that the most of the Ku-bands frequency range from 12 GHz to 17 GHz is covered, and the 3 dB-bandwidth is larger than 5 GHz thanks to these wide band optoelectronics devices.

According to the phase relationship between delay difference and wavelength difference which can be expressed as

$$\Delta\varphi = D \cdot \Delta\omega \cdot f_0 \qquad (3)$$

Where D is the average dispersion coefficient of a channel, $\Delta\omega$ is the laser wavelength change, and f_0 is the frequency of microwave signal. The delay is changing in a linear fashion with wavelength scanning at a fixed frequency of the transmit signal. Fig. 2(b) plots the time delay curves for all 16 channels beamformer, when the channel 1 in 1545 nm is used as the zero-delay reference. The designed tunable range of laser wavelength is from 1530 nm to 1560 nm, and the 16th channel has the longest DCF among all channels. As the results, the delay difference in tunning wavelength of 30 nm of every 16 channels keep almost equal intervals, which are -99.94, -47.72, 24.83, 67.58, 118.53, 174.12, 219.83, 283.9, 325.1, 389.4, 438.3, 509.3, 541.3, 598.1, 656.3, and 721.3 ps, respectively. The fabrication errors of the DCF length could be badly affecting the slope of the delays. Precisely matched the lengths of the DCF and SMF is one of the major challenges in the work. The length of the DCF is fixed, because we customize the optical fibers with DCF and SMF. The compensation of the SMF length can ensure the accuracy of the system. We splice the SMF and measure the total delays by VNA in real-time. The random phase errors, and the laser wavelength shift may cause the measuring errors. Experimental results show that this system realized expected delay requirements by designing the fiber length.

However, there are still slight deviations from the ideal linear lines in amplitude and phase. Fig. 2(c) shows the summarizing amplitude deviations from the fitting values with different input power in all 16 channels, that more than 93.75% data is within the range of ±0.25 dB, exhibiting a high linearity range from -50 dBm to 0 dBm. Fig. 2(d) summarizes the statistics of phase deviations in all channels. More than 91.48% phase random error is within the range of $\pm3.5°$. It illustrates the high degree of uniformity among 16 channels. These small deviations are due to the dynamic range of optoelectronics devices and the small fiber cutting errors. They have micro-impacts on the performance of scanning array antenna as [18], [19].

3.2 Directional Diagram and SFDR

Moreover, we assumed a 16-array-element of an antenna array with element spacing of $\lambda/2$@ 14.5 GHz applied in this up/downstream shared optical beam forming network system. Bringing the S_{21} parameters into the directional diagram equation (1), the directional diagrams which the relationship between sweeping angle θ and RF power is shown in Fig. 3(b). The beamwidth of the main lobe is less than 4.5° at 1545 nm. According to Fig. 3(b), the corresponding relationship between optical wavelength and RF beam steered angle at 14.5 GHz is shown in Fig. 3(a). When the transmit signal is at 14.5 GHz, the main lobe is oriented from $-49.3°$ to 45.9° with the wavelength scanning from 1530 nm to 1560 nm. Since the high-order dispersion of DCF cannot be neglected in a large optical wavelength range, the relationships between time delay and wavelength are not a perfectly linearity. This deviation leads to an asymmetry beam steered angle of 3.4° in the proposed system. The phase of the fiber shows a non-linear change with wavelength when the wavelength interval is too long to ignore the high order dispersion coefficient. In addition, the beam steered angle is proportional to the wavelength scanning range of the laser, which can be further improved with a wider wavelength-tunable range of the laser over C+L bands. Limited by the wavelength scanning speed of the laser, the beam switching speed will be faster with the help of a faster tunable laser. At 1540 nm, the beam angle deviations are less than 0.16° with the frequency varies from 12 GHz to 17 GHz as shown in Fig. 3(c). The optical TTD system reduces the effect of beam squint, which means the beam forming direction is nearly unchanged with the instantaneous frequency changed. Therefore, a wide instantaneous bandwidth beam forming system can be achieved without the effect of beam squint. As shown in Fig. 3(d), measurements for third order intermodulation showed the spurious free dynamic range (SFDR) of 104.58 dB·Hz$^{2/3}$ at 12 GHz,
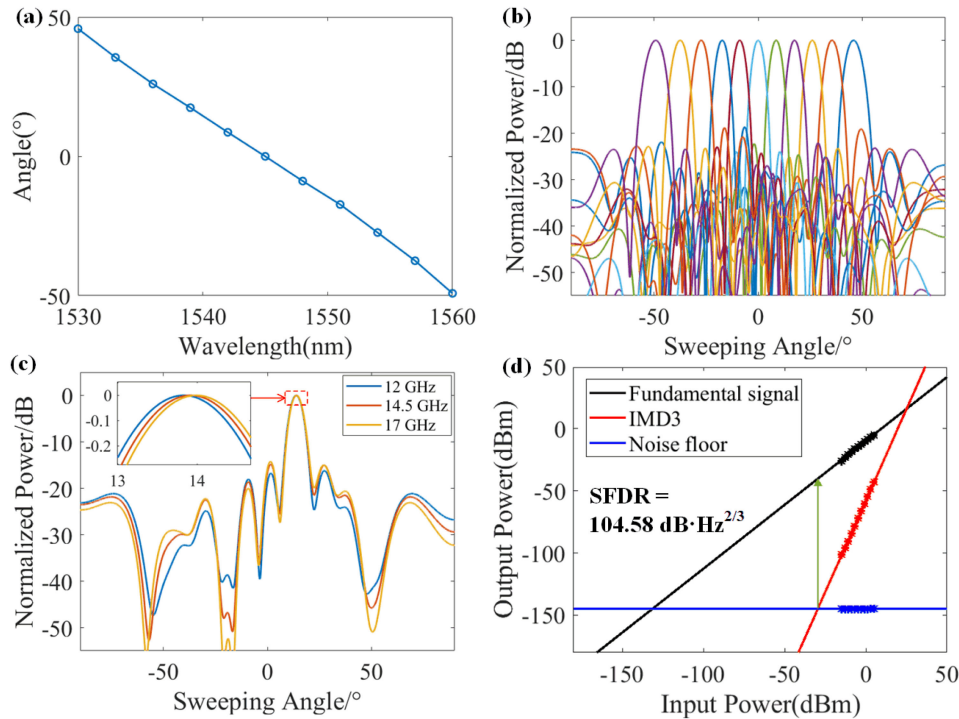
Fig. 3. (a) Directional diagram from −49.3° to 45.9° when wavelength scanning from 1530 nm to 1560nm. (b) The relationship between optical wavelength and RF beam steered angle at 14.5 GHz. (c) The beam angle deviations in the 1540 nm at different frequencies. (d) The spurious free dynamic range of this system.

which is measured using the recognized dual tone multi-frequency method. The tone-signal of 12 GHz and 12.1 GHz is set at the same power by two microwave sources (Keysight N5183B). The microwave signal generated from the PD at the frequency of 11.9 GHz, 12 GHz, 12.1 GHz, and 12.2 GHz because of the third intermodulation distortions in a large microwave signal power. With the change of the tone signal power, the power values of these four frequencies are measured by a spectrum analyzer (ESA R3182). The SFDR is determined by the fitting curve from these power values and noise floor. It is implemented by well controlled modulators' bias. Such a large SFDR indicates more clear images in detection.

3.3 Influence of Temperature Drifts and Others

The temperature control has a significant influence on the performance of the system and the life of the devices. We stimulated a series of random temperature drifts within 6°C on different channels as shown in Fig. 4. The delay of fiber τ is depended on the temperature T which can be expressed as

$$\frac{d\tau}{dT} = \frac{L}{c}\frac{dn}{dT} + \frac{n}{c}\frac{dL}{dT} \tag{4}$$

Where c is the speed of light in a vacuum, L is the fiber length, and n is the refractive index. We take the deviation of the length and refractive index with respect to temperature. According to [20], the typical values in single-mode fiber are $\frac{dn}{dT} = 1 \times 10^{-5}/°C$ and $\frac{dL}{dT} = 5.5 \times 10^{-7}m/°C$. As shown in Fig. 4(a), six groups of random temperature drifts are applied in the stimulations, which follow a uniform distribution pattern in the interval of (0, n), (n = 1, 2, 3 …6), respectively. Fig. 4(b) shows the beam direction impact of changing the temperature. The temperature drifts within 6° C
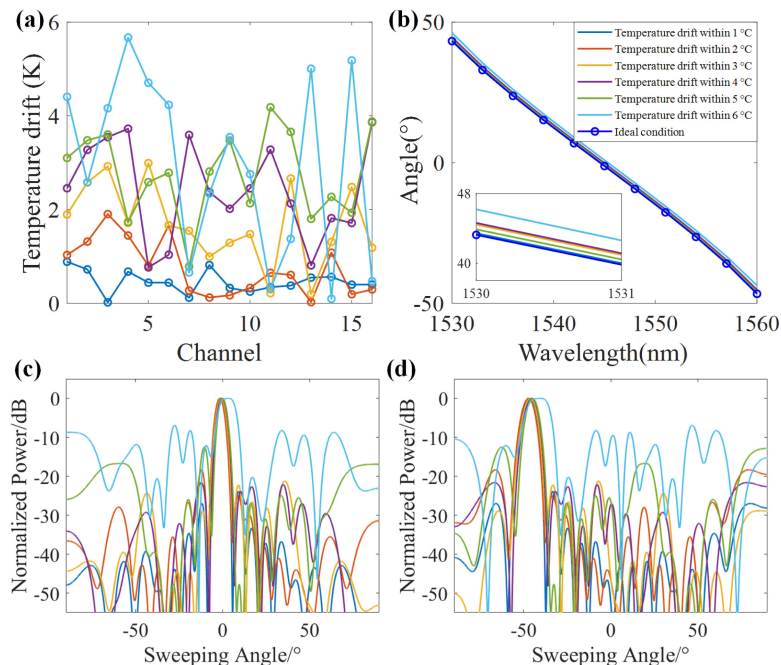
Fig. 4. The random temperature drift (a) has a significant influence on the beam squinting (b) and directional diagram at 1545 nm (c) and 1560 nm (d).

causes beam squinted of 2.9° in 1530 nm. The directional diagrams at 1545 nm and 1560 nm get worse main lobe width and sidelobe compression ratio, as shown in Fig. 4(c) and (d). Significantly, the stimulated result is just an illustration in the special condition of Fig. 4(a). In another random temperature condition, the values may be varied but the trends will not change. In a word, it is important to ensure temperature uniformity across the different channels. Thus, we take measures of heat dissipation to mitigate those effects. Part of the heat is given off by cooling fans, another part of the heat is diffused outward by directly contact the mental case. Usually, the temperature control won't cause such a large temperature difference among channels.

Interference among the upstream and downstream can affect the transceiver system performance, which is mainly governed by the performance of the optical circulators. For example, the transmit signal may leak from port 3 of the first optical circulator or return from port 2 of the second optical circulator and then convert to the receive signal directly. At present, the optical circulator, whose directivity (from port 1 to port 3) and return loss more than 50 dB is commercially available. With the help of these optical circulators or add more optical isolators, the interference will be reduced in the estimate. The proposed system is able to realize fully duplex when the wavelength of two lasers is symmetric along the center wavelength of 1545 nm. In practice, there will be a trigger signal to control the wavelength of the two lasers precisely synchronized. In addition, to construct the up/downstream shared optical beam forming network system in a miniature way, the rational distribution of such numerous devices also needs to be considered. The space distribution of the devices, the location of the electrical interface, and even the requirements of the maintenance need to take into account. Furthermore, the modular design of every channel will be easy to install and maintain if possible.

4. Conclusion

In this paper, we have experimentally demonstrated an up/downstream shared optical beam forming network based on wavelength-swept for remote phased array antenna. A shared optical TTD network minimizes the size and cost, which is made by 16 paths of variable lengths of

dispersion compensation fibers splicing with single mode fiber, and then corporate with optical circulators. The experimental results show that the proposed system provides wide bandwidth from 12 GHz to 17GHz is covered. The main lobe is oriented from $-49.3°$ to $45.9°$ and the SFDR of 104.58 dB·Hz$^{2/3}$ is achieved in this system. Besides, the optical beam forming network is not affected by external electromagnetic and temperature interference. The proposed system can easily combine with antenna remoting solutions based on microwave photonics technology, which achieves the remoted array antenna and signal processing central station. Also, this structure the proposed system verified for chip-scale integration in the future.

Acknowledgment

References

[1] D. Wake, A. Nkansah, and N. J. Gomes, "Radio over fiber link design for next generation wireless systems," *J. Lightw. Technol.*, vol. 28, no. 16, pp. 2456–2464, Aug. 2010.

[2] J. Yao, "Microwave photonics," *J. Lightw. Technol.*, vol. 27, no. 3, pp. 314–335, Feb. 2009.

[3] H. Schippers *et al.*, "Broadband optical beam forming for airborne phased array antenna," in *Proc. 2009 IEEE Aerosp. Conf.*, Big Sky, MT, USA, 2009, pp. 1–19.

[4] N. Shi, W. Li, N. Zhu, and M. L. J. C. O. Letters, "Optically controlled phase array antenna [Invited]," vol. 17, no. 5, pp. 052301–052301, May 2019.

[5] S. Pan, X. Ye, Y. Zhang, and F. Zhang, "Microwave photonic array radars," *IEEE J. Microw.*, vol. 1, no. 1, pp. 176–190, Jan. 2021.

[6] B. Howley, X. Wang, M. Chen, and R. T. Chen, "Reconfigurable delay time polymer planar lightwave circuit for an X-band phased-array antenna demonstration," *J. Lightw. Technol.*, vol. 25, no. 3, pp. 883–890, Mar. 2007.

[7] B. Jung, and J. Yao, "A two-dimensional optical true time-delay beamformer consisting of a fiber bragg grating prism and switch-based fiber-optic delay lines," *IEEE Photon. Technol. Lett.*, vol. 21, no. 10, pp. 627–629, May 2009.

[8] X. Ye, F. Zhang, and S. Pan, "Compact optical true time delay beamformer for a 2D phased array antenna using tunable dispersive elements," *Opt. Lett.*, vol. 41, no. 17, pp. 3956–3959, Sep. 2016.

[9] N. K. Srivastava, and S. K. Raghuwanshi, "Demonstration of highly steerable beamforming system incorporating a waveguide of spatially distributed fiber bragg grating," in *Proc. 2019 6th Int. Conf. Signal Process. Integr. Netw.*, 2019, pp. 367–370.

[10] H. Ito, T. Tatebe, H. Abe, and T. Baba, "Wavelength-division multiplexing si photonic crystal beam steering device for high-throughput parallel sensing," *Opt. Exp.*, vol. 26, no. 20, pp. 26145–26155, Oct. 2018.

[11] A. Kanno, P. T. Dat, and N. Yamamoto, "96-GHz Phased array system using wavelength selectable switch-based dispersion control," in *Proc. 2020 Int. Topical Meeting Microw. Photon.*, 2020, pp. 249–252.

[12] N. Shi *et al.*, "Experimental demonstration of a multi-target detection technique using an X-band optically steered phased array radar," *Opt. Exp.*, vol. 24, no. 13, pp. 14438–14450, Jun. 2016.

[13] W. Zhang, and J. Yao, "Silicon-Based integrated microwave photonics," *IEEE J. Quantum Electron.*, vol. 52, no. 1, pp. 1–12, Jan. 2016.

[14] R. Cao *et al.*, "Multi-channel 28-GHz millimeter-wave signal generation on a silicon photonic chip with automated polarization control," *J. Semicond.*, vol. 40, no. 5, May 2019, Art. no. 052301.

[15] W. Ma *et al.*, "Practical two-dimensional beam steering system using an integrated tunable laser and an optical phased array," *Appl. Opt.*, vol. 59, no. 32, pp. 9985–9994, Nov. 2020.

[16] D. Marpaung, J. Yao, and J. Capmany, "Integrated microwave photonics," *Nature Photon.*, vol. 13, no. 2, pp. 80–90, Sep. 2019.

[17] S. Li *et al.*, "Chip-Based microwave-photonic radar for high-resolution imaging," *Laser Photon. Rev.*, vol. 14, no. 10, Aug. 2020, Art. no. 1900239.

[18] L. Yaron, R. Rotman, S. Zach, and M. Tur, "Photonic beamformer receiver with multiple beam capabilities," *IEEE Photon. Technol. Lett.*, vol. 22, no. 23, pp. 1723–1725, Dec. 2010.

[19] O. Raz, S. Barzilay, R. Rotman, and M. Tur, "Submicrosecond scan-angle switching photonic beamformer with flat RF response in the C and X bands," *J. Lightw. Technol.*, vol. 26, no. 15, pp. 2774–2781, Aug. 2008.

[20] N. Shibata, S. Shibata, and T. Edahiro, "Refractive index dispersion of lightguide glasses at high temperature," *Electron. Lett.*, vol. 17, no. 8, pp. 310–311, Feb. 1981.